Moisture equilibrium of cement based materials containing slag or silica fume and exposed to repeated sorption cycles

M. Saeidpour*, L. Wadsö

Building Materials, Lund University, Lund, Sweden

Abstract

Water vapor sorption isotherms are essential data in models to predict the service life of cement based structures. This study investigates the influence of water to binder ratio (0.4, 0.5 and 0.6), and the presence of two SCMs (70% slag and 10% silica fume) on sorption isotherms, both in the hygroscopic and in the super-hygroscopic relative humidity (RH) ranges.

Desorption isotherms are in the present paper divided into different parts based on Jennings CM-II model of the C-S-H structure. The samples with silica fume and slag have higher moisture content than OPC samples, but with higher amount of gel pores and lower amount of capillary pores. At low RHs all samples have similar desorption curves and the introduction of SCMs induce only a slight increase in the BET surface area.

Keywords: Cement paste; Cement mortar; Sorption isotherms; Sorption cycles; Supplementary cementitous materials (SCMs)

1. Introduction

All physiochemical processes that are responsible for durability issues in concrete, such as carbonation, chloride initiated corrosion, sulfate attack, freeze and thaw cycles, and alkali silica reaction (ASR), are moisture dependent [1, 2], so the durability of cement and concrete structures depends on transport and sorption of moisture. To be able to predict the rates at which these processes occur~~,~~ or to prevent their occurrence, transport and sorption data are needed. Water vapor absorption and desorption isotherms are the equilibrium water contents of the material as a function of relative humidity (RH) at a constant temperature. These data are used in computer models to predict the service life of structures [3] and are essential to understand moisture distribution in cement based structures [4]. Sorption isotherms can also be used for the calculation of for example specific surface areas, and thus contribute to a better understanding of the microstructure.

The equilibrium moisture content at a certain RH is higher for materials subjected to drying than for the same material that is absorbing moisture (at the same RH). This phenomenon is referred to as sorption hysteresis and is important to take into account when modeling transport properties in materials exposed to wetting and drying cycles, such as many outdoor and indoor concrete structures [5, 6]. One example of such a structure is the surface of indoor concrete floors that are often exposed to an initial drying, followed by a wetting by the water

*Corresponding author.
Email-address: mahsa.saeidpour@byggtek.lth.se. Tel: +462227786

in applied adhesives or screeds, and finally a drying to the room climate [4]. Such a process cannot be understood without knowledge of hysteresis and scanning curves.

The first sorption isotherms on cement pastes were measured by Powers and Brownyard in 1948 (see references [7, 8]) and there are many reports on sorption isotherms of pastes, mortars and concretes made with ordinary Portland cement (OPC), see for example references [9-13]. However, these results are often difficult to compare due to a number of factors being different between studies or not well described; for example hydration conditions, aging of samples during experiments (continued hydration and/or carbonation), absorption-desorption history and method of sorption studies. For example, Hagymassy et al. [12] reported low hysteresis for hardened OPC pastes in the high RH region and almost no hysteresis at low RHs, which is in contrast with isotherms reported by Feldman and Sereda [11] and Baroghel-Bouny [13].

The hysteresis at high RHs is commonly explained by the inkbottle effect in capillary pores [14, 15], while the hysteresis at low RHs is still not fully understood. Pore collapse is described as responsible for low RH hysteresis by many authors (cf. [10, 13, 16]). However, Bazant and Bazant [17, 18] debate this and describe two mechanisms as possible responsible for low RHs hysteresis: snap-through instabilities during the filling and emptying of non-uniform nano-pores and molecular coalescence within the partially filled surface in nano-pores.

In contrast to OPC, the knowledge about sorption isotherms for materials made with blended cements is limited; such knowledge is crucial today as there is a general trend of using more blended cements with supplementary cementitous materials (SCMs) as a way to limit the CO_2 emissions associated with concrete. The presence of SCMs changes the amount and kind of hydrates formed during the hydration, especially the calcium silicate hydrate (C-S-H) that is the main product of cement hydration [19]. This changes the internal surface and pore structure, and thus the sorption and transport properties.

Few studies of sorption isotherms of cement based materials with SCMs have been published and there is still a need for systematic studies in this field. Baroghel-Bouny et al. [13] investigated sorption isotherms and hysteretic behavior of high performance (HP) cement pastes and concretes made with OPC and 10% silica fume. They performed several scanning curves from different RHs and analyzed pore size distributions with the Barrett, Joyner, Halenda (BJH) model [20]. Their results showed that HP materials had lower moisture contents at high RHs compared to normal materials, and large RH changes at high RHs induced only slight changes in moisture content [13]. De Belie et al. [21] studied the microstructure and surface area change of cement pastes in which OPC had been replaced by SCMs in different mass fractions (10% silica fume, 50% fly ash, and 50 and 85% slag). They did static and dynamic (sorption balance) water vapor and nitrogen sorption isotherms on samples with water/binder ratios (w/b) 0.35-0.5 without any specific control on carbonation. They conclude that the result of the sorption isotherm measurement is dependent on the method used. Their results showed hysteresis over the whole range of RH for all binders.

The evaluation of moisture properties of cement based materials require at least the main absorption and desorption curves of the sorption isotherm [22]. These can be measured with different techniques. The most common method is the desiccator method (see for example references [5, 10, 21]). In this method relatively large samples are equilibrated for several weeks at different vapor pressures above saturated salt solutions, and are weighed on a balance until they have reached equilibrium. This method is time consuming and needs many parallel specimens that are exposed to different RHs. In addition, the structure of the material may change during the long measurement time due to hydration and carbonation. In the present study we used the sorption balance method, in which small samples (10-100 mg) are continuously weighed on an analytical balance while exposed to an RH program. The main advantages with this technique are that the whole isotherm can be measured on a single sample in a CO_2-free environment. A measurement is comparatively quick as the external mass transfer resistance is low as the sample is exposed in a gas stream. However, each of our measurements still takes about three weeks.

In this study, the influence of w/b-ratio (0.4, 0.5 and 0.6) and the presence of two SCMs (70% slag and 10% silica fume) on the microstructure and water vapor isotherms of paste and mortar samples were studied in a systematic way. Care was taken so that the samples were exposed to the same treatment before the measurements, and the sorption balance method was used to avoid carbonation.

2. Materials

Nine pastes and six mortars with different binders have been used in this study. The binders were ordinary Portland cement OPC (CEM I), OPC with 10% silica fume, and OPC with 70% slag (CEM III). The chemical compositions of the cements and the silica fume are given in Table 1. The CEM III was premixed and the silica fume was added to the OPC as slurry. Three water/binder-ratios (w/b), 0.4, 0.5 and 0.6, for paste samples and two w/b ratios, 0.4 and 0.5, for mortar samples were used.

The mortar materials were mixed with water according to EN 196-1 and cast in a 40×10×10 cm^3 steel mold. The mold was placed in a 20 °C climate room and cooled with fans during first 24 hours of hydration to limit the temperature increase. Temperature was measured with thermocouples on the surface of the steel mold and in the center of the samples during 24 hours of hydration. The maximum temperature measured in the center was 24 °C (for samples with 10% silica fume). The samples were seal cured for 90 days at 20 °C and then crushed to pieces of approx. 5 mm. The crushed pieces were kept in sealed containers to avoid carbonation and in contact with wet cloth to become capillary saturated.

The preparation of the paste materials followed EN 196-1. The pastes were cast in cylindrical plastic bottles with 70 mm diameter and 200 mm height. After mixing, the bottles were rotated for 12 h to avoid segregation. All materials were then stored in the bottles at 20 °C. After 3-6 months of curing, the cylindrical samples were crushed to pieces of about 100 g, and these pieces were vacuum saturated. Saturated materials were stored in 100% RH in exsiccators until the measurements started.

Both mortar and paste samples were crushed to 1-2 mm pieces before being placed in a sorption balance. The measurements were done more than one year after casting. As the mortar samples were so small (20 mg), their paste content was not the same as that of the large sample from which they were taken. To be able to compare sorption isotherm measurements on pastes and mortars, the cement content of the latter were calculated from the calcium contents of the small samples as measured by Inductivity Coupled Plasma Mass Spectroscopy (ICP-MS) after the sorption measurements.

The samples for pressure plate testing were small slab shaped cement paste samples of approx. 20×15×3 mm^3 that were cut from the paste cylinders. All pressure plate samples were vacuum saturated before the tests.

Place Table 1 here

3. Experimental techniques

3.1. Water vapor sorption balance

For the sorption balance measurements approx. 20 mg of water saturated samples were placed in a DVS Advantage (Surface Measurement Systems, UK) sorption balance. In these instruments the mass of the small sample is continuously measured with an analytical balance while exposed to an RH-program. The desired RH is reached by mixing different proportions of dry and water vapor saturated nitrogen gas streams. The relative humidity of the sorption balance was validated by measurements on saturated salt solutions and found to be within 1.5% of the set values. Most measurements were made with an RH-program consisting of desorption (95-90-80-…-40-30), absorption (30-40-…-80-90-95), and desorption (95-90-80-70-...50-40-30-25-20-15-10-5-0). One measurement was made with one more absorption-desorption cycle. An example of a typical RH-program and the corresponding mass change is shown in Fig. 1. Each RH step was ended when the mass change rate was lower than 0.0001% of the initial mass per minute, or if a maximum time of 2000 min had been exceeded; except for final drying that was continued for up to 6000 min. A complete measurement for one sample – including one desorption curve, one absorption curve, and one final desorption curve to 0% RH – took approx. 20 days.

Place Fig1 here

The moisture content of the sample at equilibrium at each relative humidity was expressed as mass of water per mass of dry material. The mass for each step was curve fitted using an exponential function (Eq. 1) and then extrapolated to infinite time to evaluate the final (equilibrium) mass m_f [23].

$$m(t) = m_0 + (m_f - m_0)\exp(-k(t - t_0)) \qquad (1)$$

Here, $m(t)$ is mass of the sample (g), t is time (s), and m_0 , m_f , k and t_0 are fitting parameters. Figure 2A shows an example of measured data and the corresponding extrapolated curve using Eq. 1. Note that only the final part of the mass curve was used in the curve fitting (cf.

Fig. 2A) and that m_0 and t_0 are free fitting parameters (not the initial mass and time). The extrapolation never changes the mass change during a single step more than 10%.

Place Fig2 here

The measured mass responses after changes in the RH do in many cases not agree with what should be expected if external and internal mass transfer resistances (Fick's law) governed the gain or loss of moisture. The main deviation is that mass equilibrium is reached more slowly than would be expected from a "Fickian" behavior. This is clearly seen when the results are drawn as a function of the square root of time (Fig. 2B), as is normally done when evaluating diffusivities of slab shaped samples. The results in Fig. 2 show that although the exponential curve fit on a linear time scale looks reasonable, the mechanisms of water sorption are more complex than usually thought and true equilibrium can possibly only be reached on much longer time scales than our experiments. A detailed analysis of the kinetics of the sorption curves will be published separately.

In this study the dry mass was defined as the extrapolated mass at infinite time for the final drying at RH=0%. To avoid microstructural damage due to drying, the samples did not dry to more than 30% RH during first desorption cycle [11].

The sorption balance measurements take about three weeks each, and it has not been possible to repeat these measurements. However, our experience from this type of measurements is that the difference between repeated measurements is very much smaller than the differences between the results presented in this paper.

3.2. Pressure plate

The sorption isotherm above the hygroscopic range was measured with pressure plate instrument from Soilmoisture Equipment Corp., Santa Barbara, CA, USA [24]. Samples were vacuum saturated and placed in two different pressure cells with 3 and 1 MPa pressure, corresponding to 97.81 and 99.26% RH, respectively. In the pressure plate, a positive gas pressure ΔP (Pa) is applied to a wet specimen and water from the sample leaves through the out-flow tubes in the instrument until equilibrium is reached in the water menisci in the material. The pore radius and RH can be calculated from the pressure at equilibrium using Young-Laplace and Kelvin equations [25]. The samples were then dried at 105 °C. The moisture contents for the pressure plate and vacuum saturated samples were reported as mass of water per mass of dry sample at 105°C. The Method is described in references [24, 26].

4. Results

The sorption isotherms measured for different w/b-ratios and different binders for both cement paste and mortars are shown in Figs. 3 and 4. Figure 3 shows all measurements made in desorption-absorption-desorption and the pressure plate and vacuum saturation data. In Fig. 4 the results of a measurement that was continued for one more absorption-desorption cycle is shown. In this figure, it is also indicated in which order the sorption curves were measured. The order is the same for all results shown in Fig. 3 (for the first three sorption limbs).

Place Figs. 3 and 4 here

5. Discussion

The discussion part contains analyses of the shape of the isotherms, the influence of SCMs on the main desorption curve, the surface area, the influence of aggregates, and the shape of the sorption isotherms at high RHs.

5.1. Shape of isotherms

Figures 3 and 4 show that all desorption-absorption-desorption curves have similar qualitative appearances; however, the OPC samples absorb less moisture than the samples with silica fume and slag. Further, the curve shapes follow a complex pattern that can be summarized in the following points:

- The initial desorption above 30-40% RH is higher than the following desorption, and the level decreases for every consecutive cycle.
- All desorption curves merge at about 30-40% RH. Below this, they follow same path for the same binder.
- Desorption isotherms show a significant change in slope between 40 and 30% RH.
- Absorption isotherms show a smooth increase over the whole RH range.
- There is a significant hysteresis over the whole RH range.

We use the Jennings CM-II model [27] and results from recent studies with ^{1}H nuclear magnetic resonance (NMR) relaxometry techniques [28, 29] to describe the shape of the desorption isotherms. The CM-II model describes the C-S-H structure based on a combination of nitrogen and water vapor sorption isotherms [27]. In this model, the basic units of C-S-H are globules that have layered sheet-like structure. The size of the globules is about 4.2 nm. A number of globules make up a floc. In this structure, the water can be found between the sheets (interlayer water) and in pores of three different sizes. Pores within the globules are referred to as interglobular pores (IGP) (pore size less than 1 nm), small gel pores (SGP) (pore size 1-3 nm) are formed between the globules, and large gel pores (LGP) (pore size 3-12 nm) are formed between flocs of globules. Much larger pores are called capillary pores. With the NMR technique two well-defined pore sizes have been found (0.85 nm and 2.5 nm [28]). These correspond to interlayer pores (IGP and interlayer water) and small gel pores (SGP). Interhydrate spaces around 10 nm corresponding to large gel pores (LGP) were also found, but decreased in volume as C-S-H grows during continued hydration [28, 29]. Based on these studies we divided the desorption isotherms into four parts (the RHs are our interpretation of Fig. 1 in reference [29]):

1. From saturated conditions to 90% RH, where capillary pores are emptied.
2. From 90 to 80% RH, where interhydrate spaces dry out.
3. From 80 to 30% RH, where gel pores are emptied.
4. From 30 to 0% RH where interlayer pores in the C-S-H structure are emptied.

Note that this is a simplified qualitative analysis to avoid the complicated and uncertain BJH calculations (cf. Wu et al. [30]), and that Jennings' model was developed for OPC and the nano-structure can be different when SCMs are used. Our analysis was made on desorption curves made by combining the initial desorption, 95 to 30% RH, with the final desorption 30 to 0% RH. This was made to avoid using the first part of the second desorption, that is made under scanning (change from absorption to desorption). Figure 5 shows the amount of water in each of these classifications for the different materials.

Place fig5 here

At low RH intervals (0-30%), desorption takes place in the interlayer C-S-H pore structure [29]. It can be seen in Fig. 5 that cement based materials with different binders and different w/b have similar moisture contents. The amount of water in this RH-range is a function of the C-S-H globule's surface area, while changes in w/b-ratio and the presence of SCMs only induce almost negligible increases in moisture content. Many studies have argued that drying below 30% RH can change the structure of C-S-H [13, 31-33]; however there is only a minor difference between the first and the second desorption curves at RHs of 30% and lower in the measurement with an extra absorption-desorption cycle (Fig. 4). This indicates that if there are microstructural changes taking place during drying, these do not influence the sorption at low RH (cf. the specific surface discussed below) or the dry mass, or that they are reversible. It should be noted that there is hysteresis between absorption and desorption also in this range, but this cannot be related to the change in the microstructure of C-S-H.

Microstructural changes were investigated by Wu et al. [34] using a desorption test with resaturated samples. They observed no major difference between the first absorption isotherm and the absorption isotherm after resaturation. They found small differences in the corresponding desorption curves, but such differences can be due to that the samples were not fully saturated during the resaturation process. These results support the idea that drying at low RHs does not change the C-S-H structure or that any change in the C-S-H structure is reversible when exposed to moisture again.

In the presence of slag and silica fume the amount of gel pores (30-80% RH) is higher than for OPC samples with the same w/b-ratio. In desorption from 80 to 40% RH, the gel pores are emptied and the amount of water lost represents the size and amount of gel pores. We thus find – using Jennings' model – that the pastes made from blended cements have higher gel porosity.

For each sample, consecutive desorption curves are different above 40% RH; the first desorption is always significantly higher and qualitative different. This difference is probably due to the fact that the second desorption is in scanning from 95% RH, while the first desorption is the main desorption curve. This is also seen in Fig. 4 where the second and third desorption curves are similar, but with the third curve below the second.

We do not show calculated pore size distributions from our data as we find that calculations of such distributions are very uncertain. If the analysis is made on the absorption curve the result is very dependent on what function that is assumed for the thickness of the adsorbed layer, and if the analysis is made in desorption the pore sizes will be underestimated because of the ink-bottle effect [15]. Except for the significant decrease in moisture content during desorption between 40 and 30% RH – which could indicate the effect of necks in ink-bottle pores – the sorption isotherms are smooth and do not give support to models based on pores with only a few discrete sizes.

From 80% to 90% RH the interhydrate spaces are emptied, and above 90% the capillary pores are emptied. In both these RH ranges there is comparatively little water desorbed, and the samples with lower w/b-ratio generally loose less water than the one with higher w/b-ratio.

There is a hysteresis between absorption and desorption over the whole RH-range for all samples. The hysteresis is more significant above 40% RH and it is larger between the first desorption (main desorption) and the following absorption than in the subsequent desorption-absorption cycle. The presence of the two SCMs tested increased the hysteresis, especially the presence of 70% slag.

Figure 6 shows the hysteresis as moisture content difference between desorption and absorption for the first and the second cycles. The hysteresis has a maximum at 70% RH for both cycles, but it is lower for RH>50% and higher for RH<50% for the second cycle compared with the first. However, the first absorption is in scanning from 30% RH, while the second absorption starts from 0% RH. At RHs close to 30%, the amount of hysteresis for first cycle is affected by scanning and can therefore be underestimated. In addition, the second absorption is a scanning curve from 0% RH and at low RHs, the amount of hysteresis is probably also underestimated. It would be interesting to compare the hysteresis between the second and the third cycles, but due to the long measurement time needed for this, it has not been made in this study.

Place fig 6 here

Figure 7 shows microstructures of the pastes of OPC and OPC with 70% slag, both with same w/b-ratio of 0.4. It can be seen in Fig. 7a that there is a dense C-S-H structure around the unreacted alite, while the C-S-H structure around the slag particles is more open. Figure 7 shows three areas with dense C-S-H; in two of these areas the C_3S phase has been completely consumed.

Place fig 7 here

5.2. Surface area

The water vapor sorption data was used to calculate the specific surface area S (m^2g^{-1}) using the BET model [35]:

$$\frac{v}{v_m} = \frac{c\varphi}{(1-\varphi)(1+c\varphi-\varphi)} \quad (2)$$

Here v_m is the monolayer moisture content (g g^{-1}), v is adsorbed moisture content (g g^{-1}), c is a constant related to interaction forces between adsorbent and adsorbate, and φ is relative humidity (Pa Pa^{-1}).

In the BET model, it is assumed that in all layers except the first, the enthalpy of adsorption is equal to the enthalpy of condensation. The enthalpy of adsorption of the first layer is higher. The monolayer moisture content can be used to calculate the specific surface area using Eq. 3.

$$S = \frac{AN_A}{M_w} v_m \quad (3)$$

Here v_m is monolayer moisture content (g g^{-1}), N_A is Avogadro's constant (mol^{-1}), M_w is molar mass of water (g mol^{-1}) and A is the area (m^2) occupied by one water molecule ($1.06 \cdot 10^{-19}$ m^2). The BET analysis was made on desorption data in the range 40-0% RH. Above this RH-range, capillary condensation may take place and the BET model will then not be valid.

The monolayer moisture content and the calculated specific surface area are presented in Table 2. It can be seen in that the specific surface area increases with decreasing w/b-ratio. The presence of the two used SCMs cause an increase in specific surface area.

According to the CM-II model, the globules are fully saturated with a monolayer on the surface at 11% RH. We report moisture contents at 10% RH, which is our closest measured point to 11% RH, to compare with the monolayer moisture content calculated using BET model. There is a good agreement between these values

5.3. Sorption isotherms for mortar samples

The measured mortar isotherms were recalculated to gram water per gram paste. An example of our recalculation for OPC paste and mortar w/b=0.5 is shown in Fig. 8.

Baroghel-Bouny [13] found that the sorption isotherms of cement pastes, mortars and concrete made with the same cement paste are the same when the moisture content is given as mass of water per mass of cement. This is natural as the aggregates of mortars and concrete normally have very low sorption of water.

Our results show that the cement paste and the cement mortar isotherms look similar, but the mortars are about 2% moisture content higher than pastes for all materials at all RHs. The reason for this is that the cement paste in the mortars loses more water in the final drying to 0% RH than do the pure cement pastes. Baroghel-Bouny only dried her samples to 3% RH, so the 2% moisture content loss of water seems to take place between 3 and 0% RH. This water loss indicates that the sand actually contributes to the sorption isotherm. We therefore measured sorption isotherms of standard sand, but found that its sorption was too low to account for the significant effect that we observed.

The only major microstructural difference between cement pastes in pastes and mortars is the interfacial transition zone (ITZ), i.e., the 30-50 μm interface between sand and mortar that has different properties from the paste[36]. One possibility is that the hydrated cement phases in the ITZ are different from those in bulk paste, for example containing phases that loose large amounts of water between 3 and 0% RH. Another possibility is that nano-sized cracks take up and loose a significant amount of water in the RH-range 0-3%. However, we have not found support in the literature for this.

Place fig8 here

5.4. Sorption isotherms at high RHs

For materials that are exposed to high (superhygroscopic) moisture conditions it is of interest to measure the sorption isotherms at high and very high RHs. As concretes frequently are exposed to rain, condensation etc. we have complemented our sorption balance results with pressure plate measurements. However, such results are probably of limited value for cement pastes, as is being discussed below.

In Fig. 3 we have drawn the pressure plate and vacuum saturation results at 97.81%, 99.26% and 100% RH. However, both 100% and 99.26% are actually higher than the possible RH range [37]; isotherms of cement based materials cannot go all the way to 100% RH because of high concentrations of ions in the pore solutions. Depending on the alkalinity of the cement, the maximum RH of the pore solution is about 98-99% [37]. Exposing samples to higher RHs than the RH of the pore solution will result in condensation of water on the outside of the material and bleeding of ions from the material to the condensation droplets.

When the whole pore system is filled, the material is saturated and cannot take up more water, i.e., this state corresponds to the highest possible moisture content. A complication is that it is difficult to fully saturate cement based materials; not even vacuum saturation will fill the whole pore system. The saturation moisture content at the sorption isotherm end point is thus uncertain and depends on the saturation method used.

Figure 9 shows a schematic isotherm at high RHs. Taking the above limitations on RH and moisture content into account, the sorption isotherm ends at point 4. Below this point, the sorption isotherms can be measured with different techniques. Points 1-2 show the results of measurements in the hygroscopic region over saturated salt solutions or in a sorption balance. At higher RHs accurate equilibration through the gas phase is difficult and the highest part of the sorption isotherm is therefore measured with the pressure plate method (point 3).

The vertical dashed line in Fig. 9 shows how the moisture content can seem to increase at constant RH if external water on a specimen is included in a measurement. This can for example happen if a pressure plate measurement is made at a pressure corresponding to an RH higher than the saturation RH, resulting in accumulation of water on the outside of the saturated sample. If all such water is removed, point 4 is reached; if it is included in the weighing, a point on the dashed line will be reached.

Place Fig. 9 here

6. Conclusions

- Desorption isotherms at low RH (0-30%) for different binders and different w/b ratios are similar. An increase in w/b-ratio and/or presence of SCMs gives small increases in calculated BET surface area.
- The moisture content above 30% RH in samples with the same w/b-ratio is higher in presence of slag and silica fume than in OPC samples. The samples with silica fume and slag have higher amount of gel pores and lower amount of capillary pores than OPC samples.
- According to this study, drying at 0% RH at room temperature in a sorption balance for several days does not change the specific surface.
- Mortars showed a higher mass loss than pastes when dried at 0% RH.
- The sorption isotherm at high RHs is difficult to validate experimentally, both concerning RH and moisture content.

Acknowledgment

The research leading to these results has received funding from the European Union Seventh Framework Program (FP7/2007-2013) under grant agreement 264448. We thank Zhang Zhidong who prepared the paste material, Arnaud Muller who helped with the SEM-samples, and Lars-Olof Nilsson and members of the Nanocem consortium with whom we discussed our results.

7. References

[1] C.R. Gagg, Cement and concrete as an engineering material: An historic appraisal and case study analysis, Engineering Failure Analysis, 40 (2014) 114-140.

[2] L.O. Nilsson, On the role of moisture in degradation of concrete structures, in: 2005 International Congress - Global Construction: Ultimate Concrete Opportunities, Thomas Telford, Dundee, Scotland, United Kingdom, 2005, pp. 15 - 24.

[3] A. Aït-Mokhtar, R. Belarbi, F. Benboudjema, N. Burlion, B. Capra, M. Carcassès, J.B. Colliat, F. Cussigh, F. Deby, F. Jacquemot, T. de Larrard, J.F. Lataste, P. Le Bescop, M. Pierre, S. Poyet, P. Rougeau, T. Rougelot, A. Sellier, J. Séménadisse, J.M. Torrenti, A. Trabelsi, P. Turcry, H. Yanez-Godoy, Experimental investigation of the variability of concrete durability properties, Cement and Concrete Research, 45 (2013) 21-36.

[4] M.S. Åhs, Sorption scanning curves for hardened cementitious materials, Construction and Building Materials, 22 (2008) 2228-2234.

[5] V. Baroghel-Bouny, Water vapour sorption experiments on hardened cementitious materials. Part II: Essential tool for assessment of transport properties and for durability prediction, Cement and Concrete Research, 37 (2007) 438-454.

[6] T.M. Chrisp, W.J. McCarter, G. Starrs, P.A.M. Basheer, J. Blewett, Depth-related variation in conductivity to study cover-zone concrete during wetting and drying, Cement and Concrete Composites, 24 (2002) 415-426.

[7] H.J.H. Brouwers, The work of Powers and Brownyard revisited: Part 1, Cement and Concrete Research, 34 (2004) 1697-1716.

[8] H.J.H. Brouwers, The work of Powers and Brownyard revisited: Part 2, Cement and Concrete Research, 35 (2005) 1922-1936.

[9] R. Badmann, N. Stockhausen, M.J. Setzer, The statistical thickness and the chemical potential of adsorbed water films, Journal of Colloid and Interface Science, 82 (1981) 534-542.

[10] R.M. Espinosa, L. Franke, Influence of the age and drying process on pore structure and sorption isotherms of hardened cement paste, Cement and Concrete Research, 36 (2006) 1969-1984.
[11] R.F. Feldman, P.J. Sereda, A model for hydrated Portland cement paste as deduced from sorption-length change and mechanical properties, Matériaux et Constructions, 1 (1968) 509-520.
[12] J. Hagymassy Jr, I. Odler, M. Yudenfreund, J. Skalny, S. Brunauer, Pore structure analysis by water vapor adsorption. III. Analysis of hydrated calcium silicates and portland cements, Journal of Colloid and Interface Science, 38 (1972) 20-34.
[13] V. Baroghel-Bouny, Water vapour sorption experiments on hardened cementitious materials: Part I: Essential tool for analysis of hygral behaviour and its relation to pore structure, Cement and Concrete Research, 37 (2007) 414-437.
[14] S.J. Gregg, K.S.W. Sing, Adsorption Surface Area and Porosity, Second ed., ACADEMIC PRESS INC, 1982.
[15] R.M. Espinosa, L. Franke, Inkbottle Pore-Method: Prediction of hygroscopic water content in hardened cement paste at variable climatic conditions, Cement and Concrete Research, 36 (2006) 1954-1968.
[16] J.J. Thomas, A.J. Allen, H.M. Jennings, Structural Changes to the Calcium–Silicate–Hydrate Gel Phase of Hydrated Cement with Age, Drying, and Resaturation, Journal of the American Ceramic Society, 91 (2008) 3362-3369.
[17] Z.P. Bažant, M.Z. Bazant, Theory of sorption hysteresis in nanoporous solids: Part I: Snap-through instabilities, Journal of the Mechanics and Physics of Solids, 60 (2012) 1644-1659.
[18] M.Z. Bazant, Z.P. Bažant, Theory of sorption hysteresis in nanoporous solids: Part II Molecular condensation, Journal of the Mechanics and Physics of Solids, 60 (2012) 1660-1675.
[19] B. Lothenbach, K. Scrivener, R.D. Hooton, Supplementary cementitious materials, Cement and Concrete Research, 41 (2011) 1244-1256.
[20] E. Barrett, L. Joyner, P. Halenda, The Determination of Pore Volume and Area Distributions in Porous Substances. I. Computations from Nitrogen Isotherms, J Am Chem Soc, 73 (1951) 373-380.
[21] N. De Belie, J. Kratky, S. Van Vlierberghe, Influence of pozzolans and slag on the microstructure of partially carbonated cement paste by means of water vapour and nitrogen sorption experiments and BET calculations, Cement and Concrete Research, 40 (2010) 1723-1733.
[22] Z. Zhang, M. Thiéry, V. Baroghel-Bouny, A review and statistical study of existing hysteresis models for cementitious materials, Cement and Concrete Research, 57 (2014) 44-60.
[23] H.H. Willems, K.B. Van Der Velden, A gravimetric study of water vapour sorption on hydrated cement pastes, Thermochimica Acta, 82 (1984) 211-220.
[24] A. Cloutier, Y. Fortin, Moisture content—water potential relationship of wood from saturated to dry conditions, Wood SciTechnol, 25 (1991) 263-280.
[25] W. Thomson, LX. On the equilibrium of vapour at a curved surface of liquid, Philosophical Magazine Series 4, 42 (1871) 448-452.
[26] M. Fredriksson, L. Wadsö, P. Johansson, Small resistive wood moisture sensors: a method for moisture content determination in wood structures, Eur J Wood Prod, 71 (2013) 515-524.
[27] H.M. Jennings, Refinements to colloid model of C-S-H in cement: CM-II, Cement and Concrete Research, 38 (2008) 275-289.
[28] A.C.A. Muller, K.L. Scrivener, A.M. Gajewicz, P.J. McDonald, Densification of C–S–H Measured by 1H NMR Relaxometry, The Journal of Physical Chemistry C, 117 (2012) 403-412.
[29] A.C.A. Muller, K.L. Scrivener, A.M. Gajewicz, P.J. McDonald, Use of bench-top NMR to measure the density, composition and desorption isotherm of C–S–H in cement paste, Microporous and Mesoporous Materials, 178 (2013) 99-103.
[30] M. Wu, B. Johannesson, M. Geiker, Application of water vapor sorption measurements for porosity characterization of hardened cement pastes, Construction and Building Materials, 66 (2014) 621-633.
[31] R.F. Feldman, Sorption and Length-change Scanning Isotherms of Methanol and Water on Hydrated Portland Cement, Division of Building Research, National Research Council, 1970.
[32] H.M. Jennings, A model for the microstructure of calcium silicate hydrate in cement paste, Cement and Concrete Research, 30 (2000) 101-116.
[33] J.J. Thomas, H.M. Jennings, A colloidal interpretation of chemical aging of the C-S-H gel and its effects on the properties of cement paste, Cement and Concrete Research, 36 (2006) 30-38.

[34] M. Wu, B. Johannesson, M. Geiker, A study of the water vapor sorption isotherms of hardened cement pastes: Possible pore structure changes at low relative humidity and the impact of temperature on isotherms, Cement and Concrete Research, 56 (2014) 97-105.
[35] S. Brunauer, P.H. Emmett, E. Teller, Adsorption of Gases in Multimolecular Layers, Journal of the American Chemical Society, 60 (1938) 309-319.
[36] P.R. Rangaraju, J. Olek, S. Diamond, An investigation into the influence of inter-aggregate spacing and the extent of the ITZ on properties of Portland cement concretes, Cement and Concrete Research, 40 (2010) 1601-1608.
[37] P.L. J. Castro, F. Rajabipour, R. Henkensiefken, and J. Weiss, Internal Curing: Discussion of the Role of Pore Solution on Relative Humidity Measurements and Desorption of Lightweight Aggregate (LWA), ACI, 270 (2010) 89-100.

Figure captions

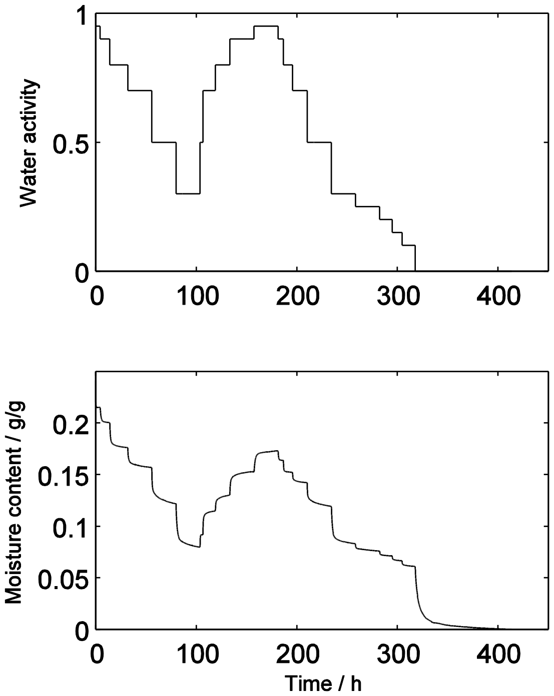

Figure 1. Typical relative humidity program and the sample response for a sample of OPC paste with w/b-ratio 0.5.

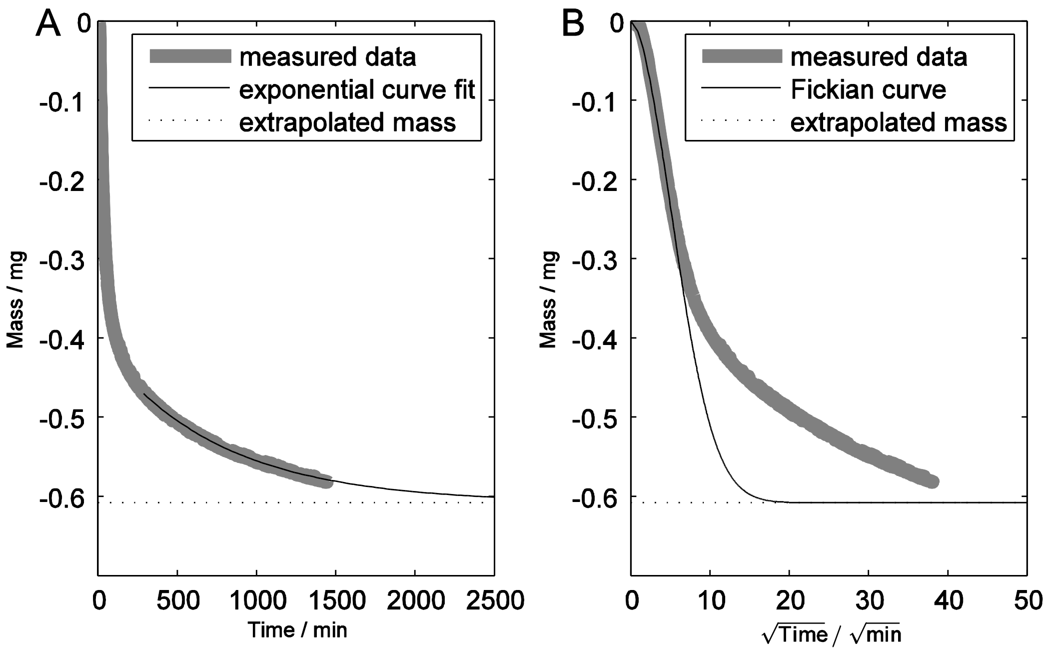

Figure 2. An example of the mass change after an RH-step (A): as function of time and (B): as function of the square root of time, The gray line is the measured data, the black line is an

exponential fitted curve in (A) and a simulated Fickian curve in (B), and the dashed line is the final (equilibrium) value found from the exponential curve fit.

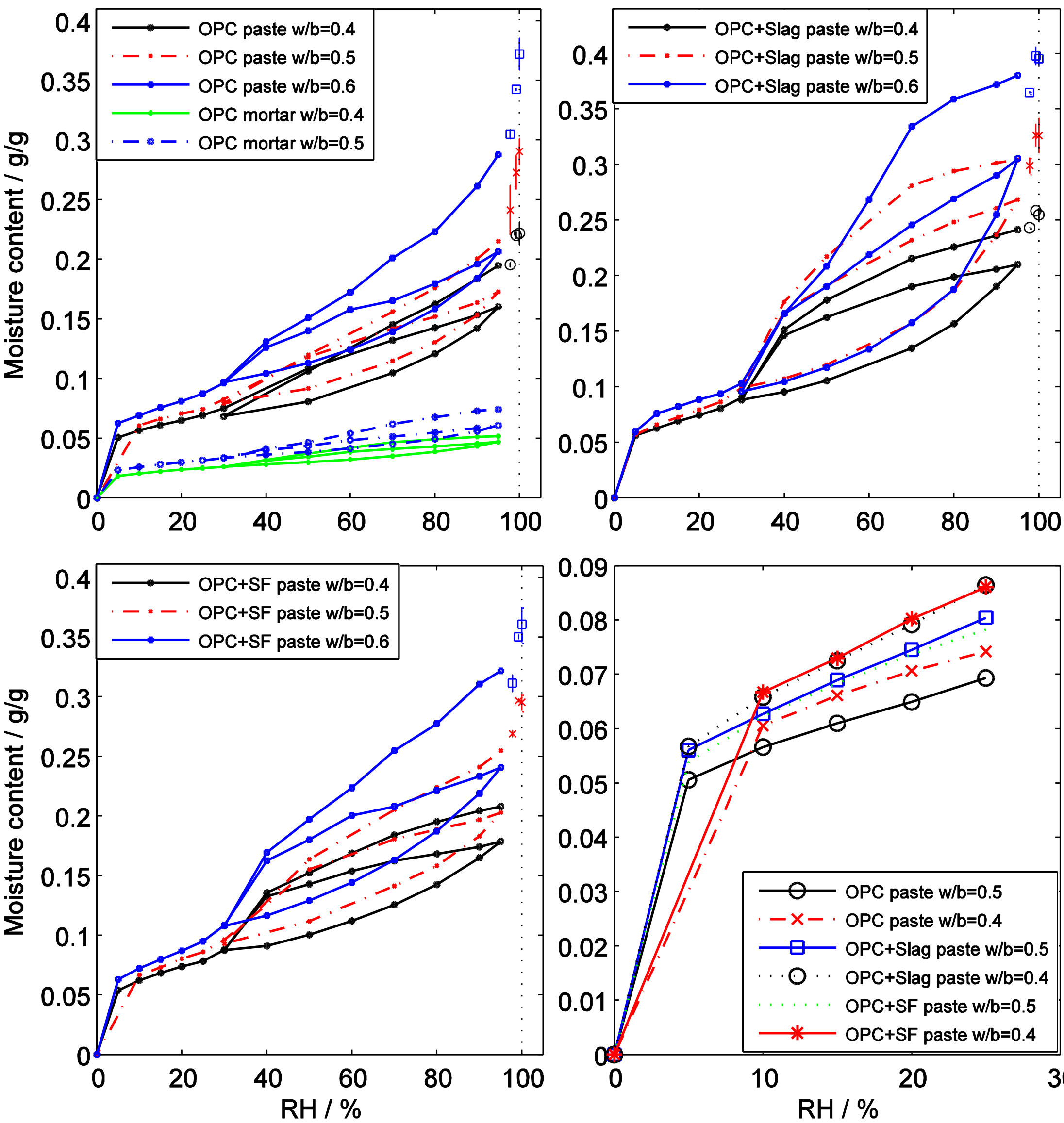

Figure 3. The sorption isotherms of cement paste and mortars with different w/b-ratios and different binders. The data connected by lines are from the sorption balance measurements. The three data points shown at high RHs are the pressure plate results for 97.81 and 99.26 % RH, and the vacuum saturation moisture content (drawn at 100% RH). These are drawn with the same color as the corresponding sorption balance measurement. The error bars for these points are the standard deviation of the three measurements made for each case (the sorption balance measurements were not repeated). The lower right diagram shows the paste results for w/b-ratios 0.4 and 0.5 in the low RH range.

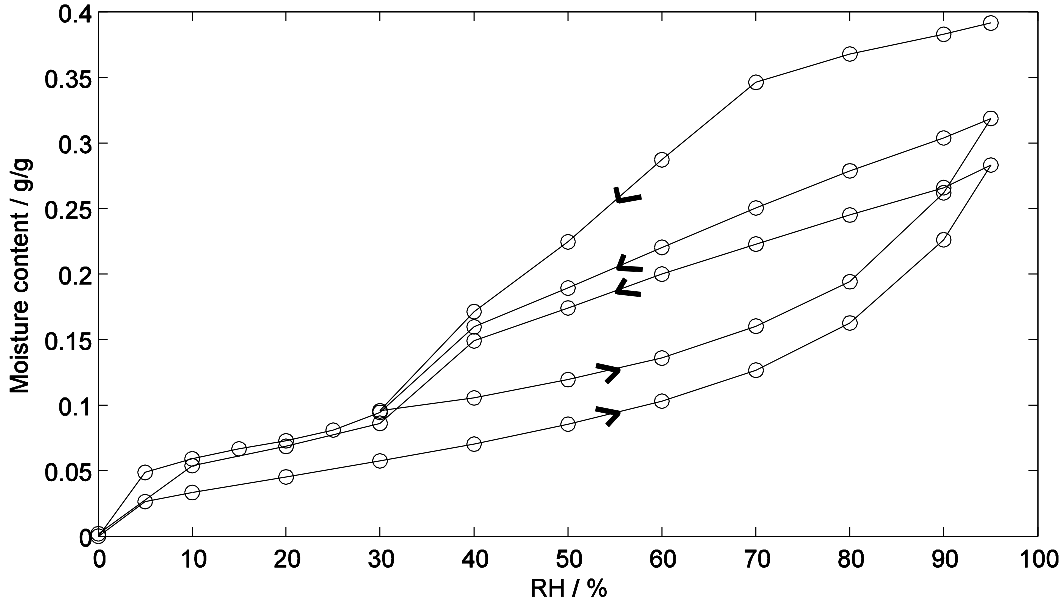

Figure 4. Sorption isotherm for OPC with 70% slag w/b-ratio 0.6 paste. Note that there is no 5% RH measurement for the final desorption.

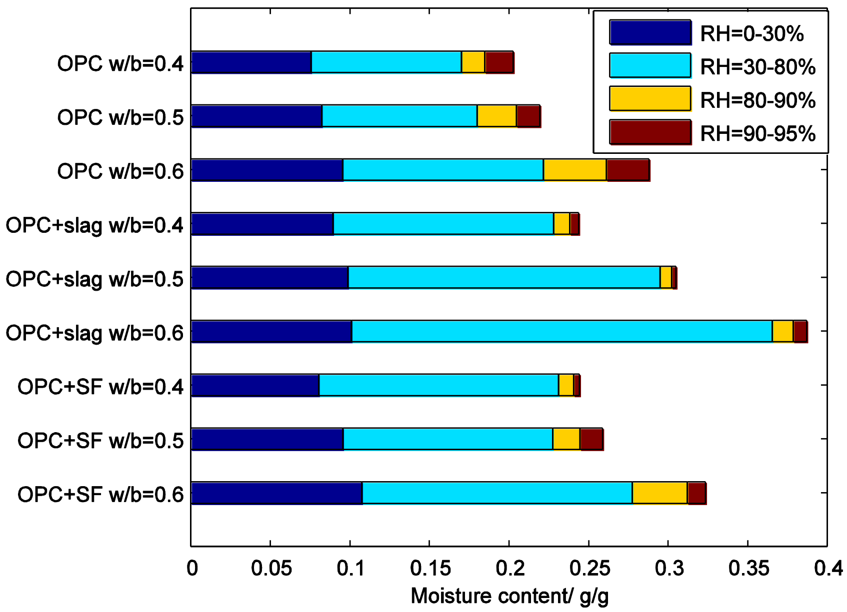

Figure 5. Amount of water desorbed in each RH interval for different cement paste samples. Data is from sorption balance measurements only.

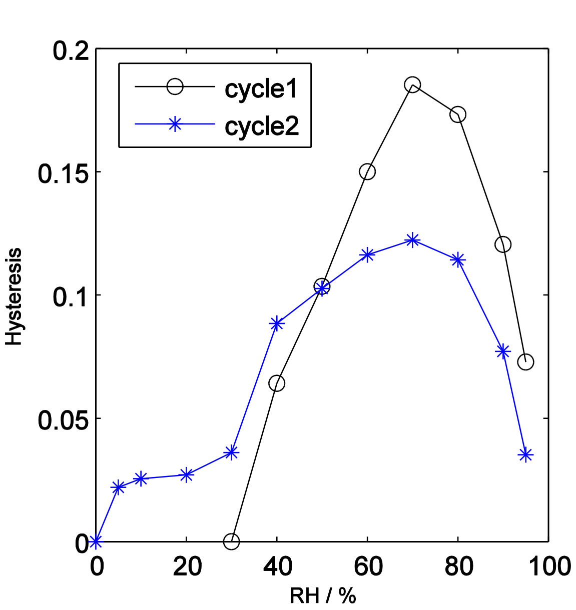

Figure 6. The hysteresis calculated for first and second cycle of sorption measurement shown in fig. 4.

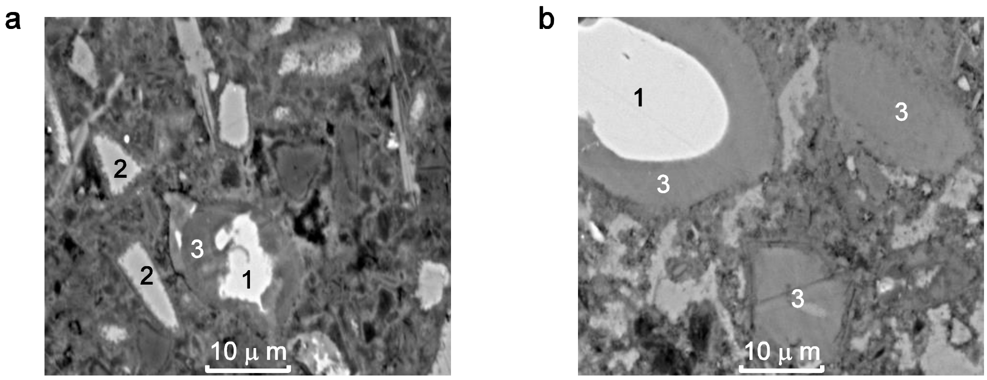

Figure 7. SEM-BSE images of two of the pastes used in the present study. a. OPC with slag b. OPC. Three phases are shown: unreacted alite (C_3S) (1), unreacted slag (2), and C-S-H (3).

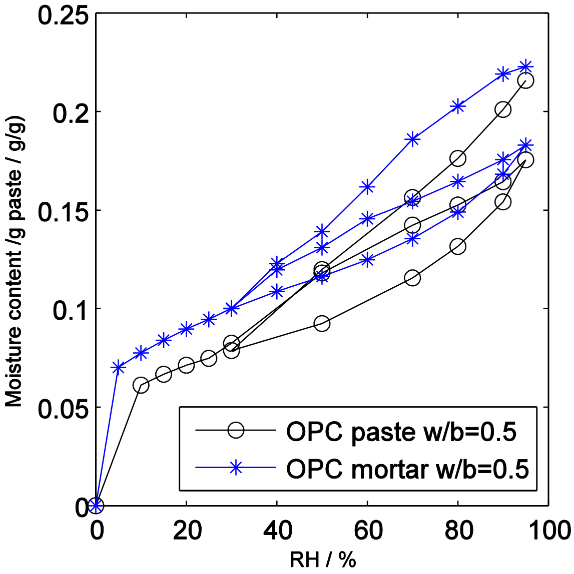

Figure 8. The recalculated sorption isotherm for cement mortar to gram water per gram paste and the paste isotherm for OPC with w/b-ratio 0.5.

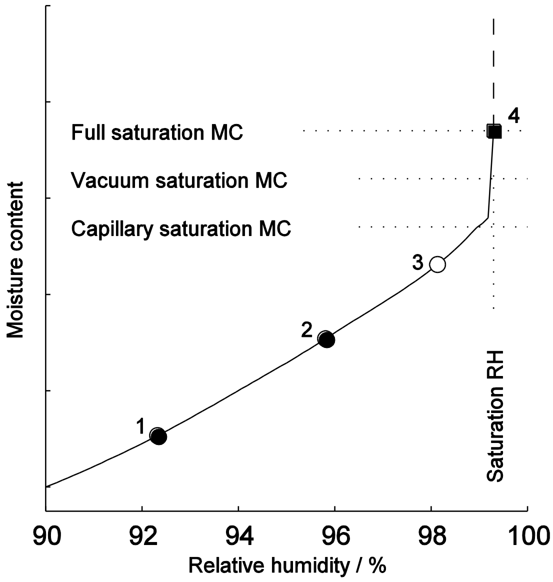

Figure 9. Schematic sorption isotherm for cement based materials. Points 1 and 2 can be measured with a sorption balance or with the saturated salt solution method; point 3 can be measured with the pressure plate method; point 4 corresponds to a filled pore system.

Tables

Table 1. Chemical composition of the used materials.

Chemical analysis XRF (%)	CEM I 32.5R	CEM III/B 42.5 N	Silica fume
SiO_2	20.3	29.2	98.7
Al_2O_3	5.6	8.9	0.31
Fe_2O_3	2.4	1.2	0.02
CaO	63.4	48	0.15
MgO	1.6	4.8	0.04
SO_3	2.9	2.6	-
LOI	2.1	1.4	0.47
Slag content	-	69.9	-

Table 2. Monolayer moisture content (v_m) and specific surface area (S) calculated from the BET model, and the measured moisture content at 10% RH (desorption).

sample	v_m (%)	S (m^2g^{-1})	Moisture content at RH=10% (%)
OPC paste w/b=0.4	5.3	187	5.7
OPC paste w/b=0.5	5.8	203	6.1
OPC paste w/b=0.6	6.7	236	6.9
OPC mortar w/b=0.4	1.9	65	2.5
OPC mortar w/b=0.5	2.4	83	2.6
OPC+slag paste w/b=0.4	6.3	222	6.3
OPC+slag paste w/b=0.5	7	246	6.6
OPC+slag paste w/b=0.6	7.3	255	7.7
OPC+slag mortar w/b=0.4	2.2	77	2.3
OPC+slag mortar w/b=0.5	2	70	2.1
OPC+SF paste w/b=0.4	6.3	219	6.2
OPC+SF paste w/b=0.5	6.9	242	6.7
OPC+SF paste w/b=0.6	7.7	268	7.3
OPC+SF mortar w/b=0.4	2.7	94	2.7
OPC+SF mortar w/b=0.5	2.7	95	2.8